# Supporting Information

## Spatial Modulation of Triphenylamine Donors in Covalent Organic Frameworks for Enhanced Photocatalytic Hydrogen Evolution

Na Qin,[a] Mengfei Wang,[a] Ke Chen,[a] Yaxiong Huo,[a] Jing Liu,[a] Yanjie Wang,[a,c]* Hualei Zhang,[b]* Liwei Mi[c]*

[a] Center for Advanced Materials Research, School of Materials Electronics and Energy Storage, Zhongyuan University of Technology, Zhengzhou 450007, P. R. China.

[b] College of Chemistry, Zhengzhou University, Zhengzhou 450001, P. R. China.

[c] Yaoshan Laboratory, Pingdingshan University, Pingdingshan 467000, P. R. China.

*Corresponding author. wangyj6527@zut.edu.cn, hualeizhang@zzu.edu.cn, mlwzzu@163.com.

**Contents**

## Section 1. Methods and Materials

### Chemicals

2,5,8,11-tetrakis(4-aminophenyl)perylene, *N,N,N′,N*-tetrakis(4-formylphenyl)benzidine, 5',5'''-bis(4-formylphenyl)-[1,1':3',1'':4'',1''':3''',1''''-quinquephenyl]-4,4''''-dicarbaldehyde and 5'-(4-(bis(4-formylphenyl)amino)phenyl)-[1,1':3',1''-terphenyl]-4,4''-dicarbaldehyde were purchased from Yanshen Technology Co., Ltd. Acetic acid (AcOH), *o*-dichlorobenzene (*o*-DCB), *n*-butanol, tetrahydrofuran (THF) and methanol (MeOH) were from Aladdin. All chemicals were used without further purification.

### Synthesis of PY-$(TPA)_2$-COF

A Pyrex tube was charged with 2,5,8,11-tetrakis(4-aminophenyl)perylene (PY, 15.41 mg, 0.025 mmol), *N,N,N′,N*-tetrakis(4-formylphenyl)benzidine ($(TPA)_2$, 15.01 mg, 0.025 mmol), *o*-DCB (0.50 mL), *n*-BuOH (0.50 mL), and 6 M AcOH (0.10 mL). The mixture was heated at 120 °C for 3 days. Upon completion, the reaction mixture was washed with THF and MeOH. The resulting solid was dried *in vacuo* at 75 °C for 3 h to afford the product PY-$(TPA)_2$-COF in 92% yield.

### Synthesis of PY-TPA-COF

A Pyrex tube was charged with 2,5,8,11-tetrakis(4-aminophenyl)perylene (PY, 14.63 mg, 0.025 mmol), 5'-(4-(bis(4-formylphenyl)amino)phenyl)-[1,1':3',1''-terphenyl]-4,4''-dicarbaldehyde (TPA, 15.42 mg, 0.025 mmol), *o*-DCB (0.5 mL), *n*-BuOH (0.5 mL), and 6 M AcOH (0.10 mL). The mixture was heated at 120 °C for 3 days. Upon completion, the reaction mixture was sequentially washed with THF and MeOH. The resulting solid was dried in vacuo at 75 °C for 3 h to afford the product PY-TPA-COF in 91% yield.

### Synthesis of PY-BFQ-COF

A Pyrex tube was charged with 2,5,8,11-tetrakis(4-aminophenyl)perylene (PY, 15.41 mg, 0.025 mmol), 5',5'''-bis(4-formylphenyl)-[1,1':3',1'':4'',1''':3''',1''''-quinquephenyl]-

4,4""-dicarbaldehyde (BFQ, 16.16 mg, 0.025 mmol), *o*-DCB (0.50 mL), *n*-BuOH (0.50 mL), and 6 M AcOH (0.10 mL). The mixture was heated at 120 °C for 3 days. Upon completion, the reaction mixture was sequentially washed with THF and MeOH. The resulting solid was dried in vacuo at 75 °C for 3 h to afford the product PY-BFQ-COF in 90% yield.

**Characterization**

Powder X-ray diffraction (PXRD) patterns were acquired using a Bruker D8 Advance diffractometer (Ni-filtered Cu-Kα radiation, 40 kV, 40 mA). Transmission electron microscopy (TEM) analysis was performed on a JEOL JEM-2100 plus instrument operating at 200 kV. High-angle annular dark-field scanning TEM (HAADF-STEM), high-resolution STEM (HR-STEM), and STEM-energy dispersive X-ray spectroscopy (STEM-EDS) elemental mapping were conducted using an aberration-corrected Xplore TEM system at 200 kV. Nitrogen adsorption-desorption isotherms at 77 K were measured on a Micromeritics 3Flex analyzer; prior to analysis. Surface morphologies were characterized by field-emission scanning electron microscopy (FE-SEM, ZEISS Merlin Compact), and elemental composition was determined with an Elementar Vario EL cube analyzer. X-ray photoelectron spectroscopy (XPS, Thermo Scientific K-Alpha) was employed to analyze surface chemical states. Fourier transform infrared (FT-IR) spectra were recorded on a Thermo Fisher Nicolet iS50 spectrometer. Solid-state $^{13}C$ cross-polarization magic angle spinning ($^{13}C$ CP/MAS) nuclear magnetic resonance (NMR) spectra were obtained using a Bruker Advance 600 MHz spectrometer. Thermogravimetric analysis (TGA) was performed under $N_2$ atmosphere on a NETZSCH 209F1 instrument, with samples heated from 30 to 800 °C at 10 °C $min^{-1}$. Surface wettability was assessed via contact angle measurements (DSA-100 goniometer). Optical properties were evaluated by ultraviolet-visible diffuse reflectance spectroscopy (UV–vis DRS, PerkinElmer Lambda 950). Steady-state photoluminescence (PL) spectra were collected using a PerkinElmer LS55 spectrophotometer, while time-resolved PL measurements utilized an Edinburgh Instruments FLS 980 spectrometer.

All electrochemical measurements were performed using a CHI760E workstation. Photocurrent responses were recorded under illumination using a conventional three-electrode configuration: indium-tin-oxide (ITO) glass as the working electrode substrate, platinum wire as the counter electrode, and Ag/AgCl as the reference electrode. For working electrode preparation, 5 mg of sample was sonicated in 0.5 mL $H_2O$ with 25 μL Nafion to form a homogeneous slurry. This suspension was coated onto a Scotch tape-masked ITO slide. After overnight drying, electrical contact was established using conductive tape to attach a copper wire. Photocurrent experiments utilized 0.2 M aqueous $Na_2SO_4$ electrolyte and a 300 W Xe lamp light source (Beijing Perfectlight, PLS-SXE300D) with a 420 nm cut-off filter. Electrochemical impedance spectroscopy (EIS) and Mott–Schottky analysis were conducted using the same three-electrode configuration.

**Photocatalytic $H_2$ evolution**

Photocatalytic water splitting reactions under visible-light irradiation were conducted in a sealed three-necked glass flask (schematic of the reaction setup shown below). The reaction solution was kept steadily at 10 °C by circulating cooling water. All COF photocatalysts adopted in this work were solid crystalline powder compounds, and the $H_2$ evolution reaction was implemented in a solid-liquid heterogeneous reaction system. Typically, 2 mg of the as-prepared solid COF photocatalyst, with $H_2PtCl_6 \cdot 6H_2O$ added as the Pt precursor (to give 1 wt% Pt loading, denoted as 1% Pt), was dispersed in 50 mL of liquid 0.10 M ascorbic acid (AA) solution contained in the reaction reactor. Prior to illumination, the whole closed system was purged with nitrogen to completely remove residual air, then sealed for reaction. Photocatalytic reactions were carried out in a custom-designed closed gas circulation system, and proceeded under continuous stirring during irradiation with a 300 W Xe lamp (PLS-SXE300, Beijing Perfect Light Technology Co., Ltd.) equipped with a 420 nm cut-off filter. The amount of evolved $H_2$ was quantified and monitored online using a gas chromatograph (SHENFEN GC 9600, equipped with MS-5A column, TCD detector, and argon as carrier gas). Photocatalytic $H_2$ production was tested in both NaCl

solutions (0.06-0.12 M, as seawater simulants) and natural seawater (3.25% w/v salt content from Bohai Sea) to assess the activity of the prepared COFs.

Photograph of the equipment setup for photocatalytic $H_2$ evolution experiments is provided below:

The apparent quantum efficiency (AQE) was calculated as: AQE= 2M/Np×100%，where M is the amount of hydrogen molecules and Np represents the incident photons.

**Recyclability experiment of PY-$(TPA)_2$-COF for photocatalytic $H_2$ evolution**

After each 4 h of photocatalytic reaction, PY-$(TPA)_2$-COF was collected by centrifugation, washed with ethanol and deionized water, and dried for subsequent reuse. This recycling procedure was repeated for different cycles under different reaction media. Notably, such recyclability tests were separately carried out in both pure water system and salt-containing seawater system, so as to evaluate its reusability under ordinary and salt-containing practical conditions.

**Calculation details**

All spin-polarized density functional theory (DFT) calculations were conducted using first-principles methodology.[1] The Perdew–Burke–Ernzerhof generalized gradient approximation (GGA) functional was employed, combined with the Semicore Pseudopotential (DSPP) method and double numerical basis sets including polarization functions (DNP).[2,3] Dispersion interactions were incorporated via the Grimme scheme (DFT-D correction).[4] The convergence criteria were set as follows: self-consistent field (SCF) electronic energy tolerance at $1.0 \times 10^{-7}$ Ha, and geometry

optimization thresholds of $1.0 \times 10^{-7}$ Ha (energy), 0.001 Ha·Å$^{-1}$ (force), and 0.001 Å (displacement). The free energy (*G*) for each reaction step was calculated as:

$$G=E+E_{ZPE}-TS$$

where E denotes the total energy, $E_{ZPE}$ denotes the zero-point energy, S denotes the entropy change, and T denotes the temperature.

The reaction energy (ΔG) of intermediates was defined as:

$$\Delta G=G_i-G_{reactant}$$

with $G_i$ and $G_{reactant}$ representing the free energies of intermediate i and reactants, respectively.

## Section 2. Supporting Figures

**Figure S1.** SEM images of (a) PY-$(TPA)_2$-COF, (b) PY-TPA-COF and, (c) PY-BFQ-COF.

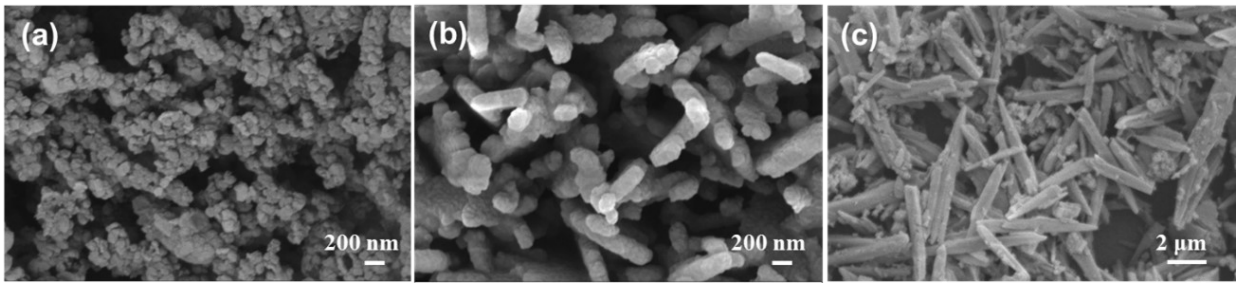

**Figure S2.** EDS mapping images of PY-$(TPA)_2$-COF.

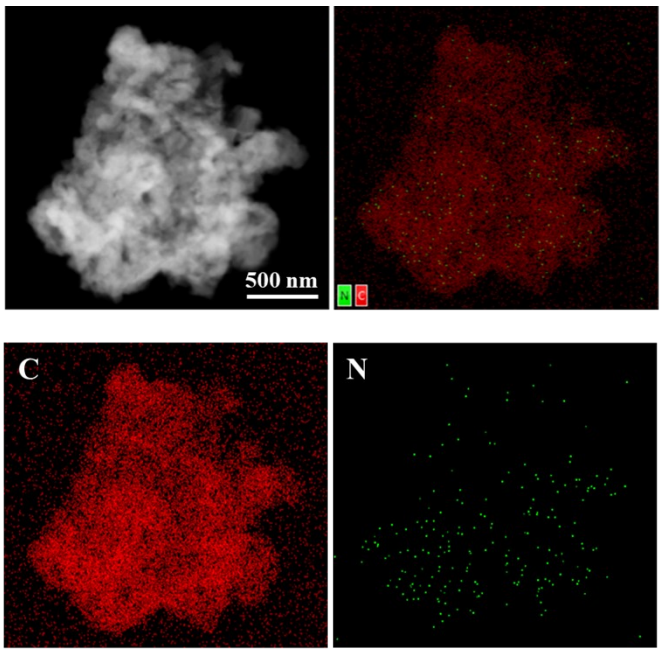

**Figure S3.** EDS mapping images of PY-TPA-COF.

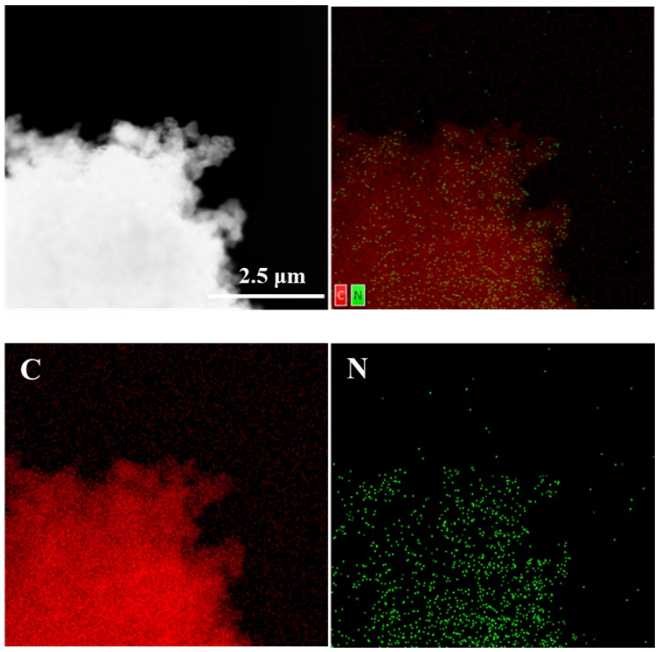

**Figure S4.** EDS mapping images of PY-BFQ-COF.

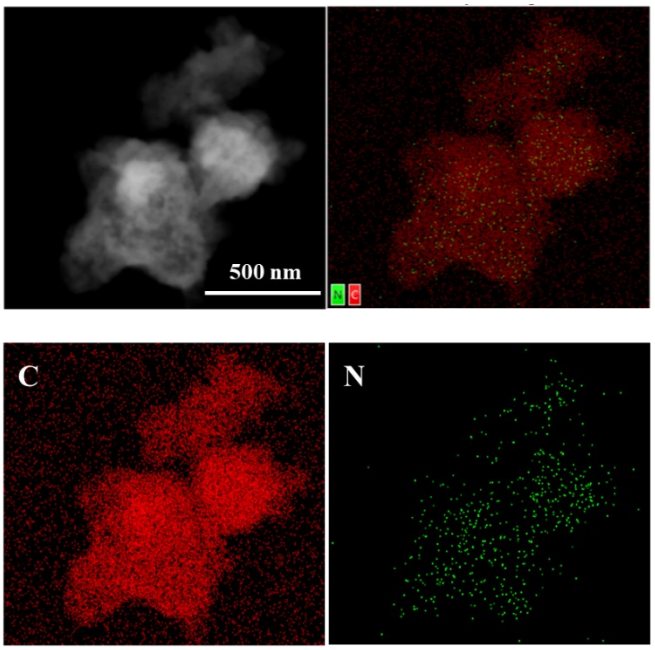

**Figure S5**. Calculated stacking energy ($E_d$) for the AA-stacking configuration of (a) PY-$(TPA)_2$-COF, (b) PY-TPA-COF, and (c) PY-BFQ-COF.

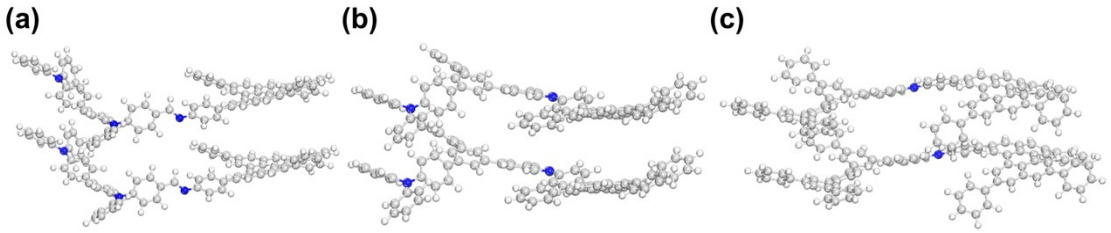


**$E_d$ = 0.53 eV** **$E_d$ = 0.73 eV** **$E_d$ = 0.98 eV**

**Figure S6.** FT-IR spectra of the monomer and PY-$(TPA)_2$-COF.

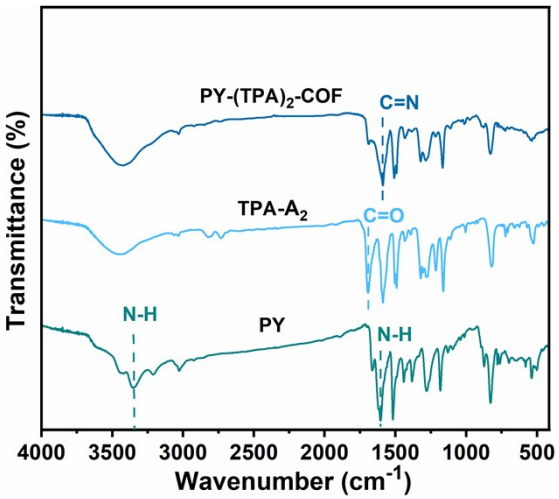

**Figure S7.** FT-IR spectra of the monomer and PY-TPA-COF.

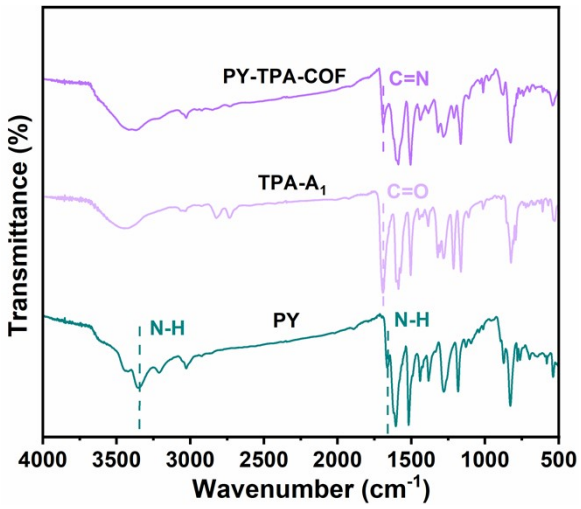

**Figure S8.** FT-IR spectra of the monomer and PY-BFQ-COF.

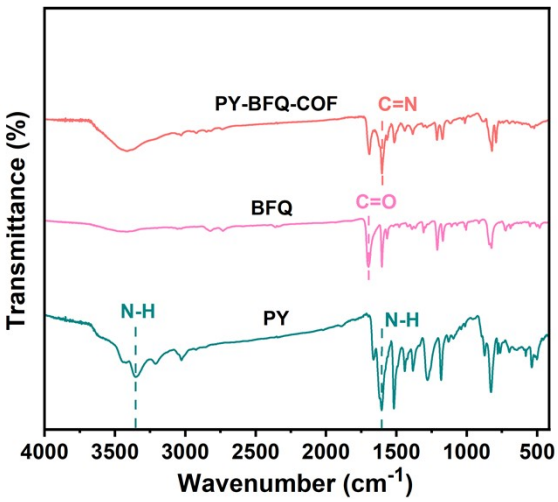

**Figure S9.** $^{13}C$ CP-MAS solid-state NMR spectra for (a) PY-$(TPA)_2$-COF, (b) PY-TPA-COF, and (c) PY-BFQ-COF.

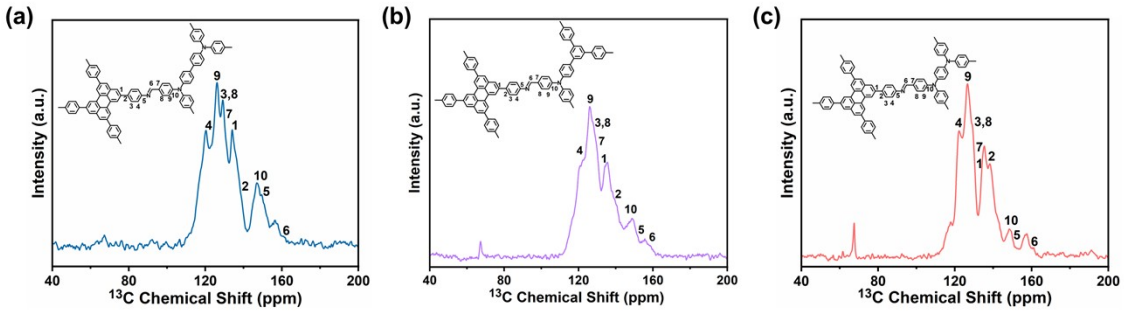

**Figure S10.** N 1s spectrum of PY-$(TPA)_2$-COF.

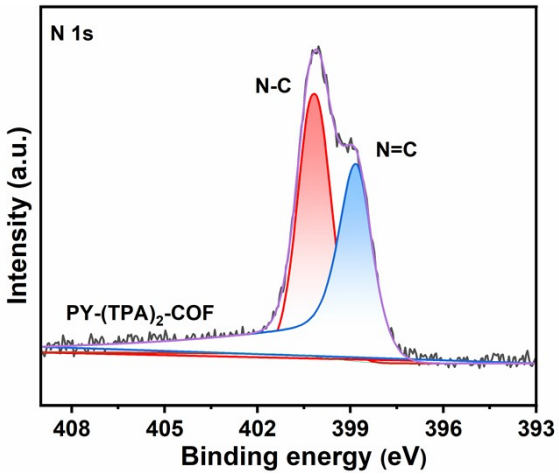

**Figure S11.** N 1s spectrum of PY-TPA-COF.

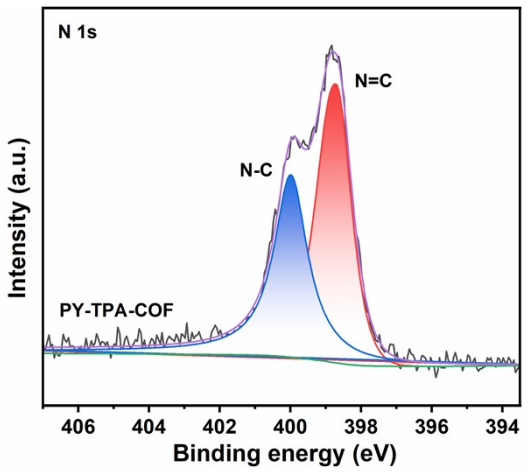

**Figure S12.** N 1s spectrum of PY-BFQ-COF.

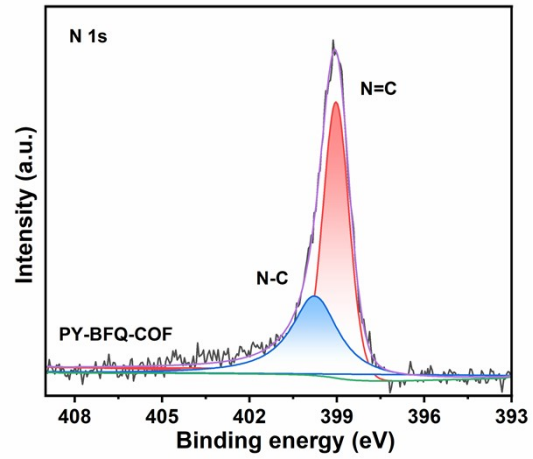

**Figure S13.** The TGA curves of PY-$(TPA)_2$-COF, PY-TPA-COF, and PY-BFQ-COF.

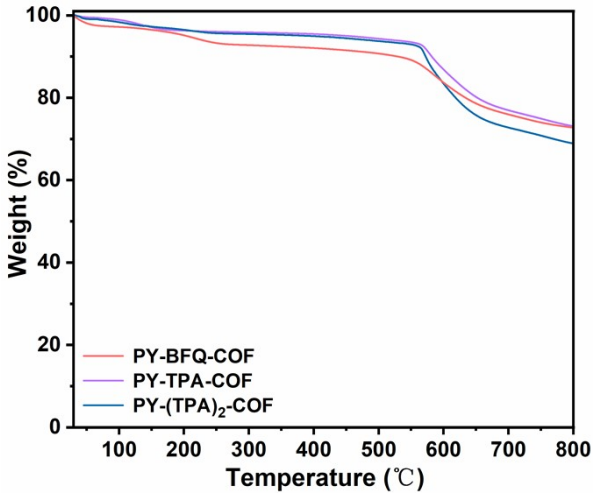

**Figure S14.** Mott–Schottky plots of (a) PY-$(TPA)_2$-COF, (b) PY-TPA-COF and (c) PY-BFQ-COF.

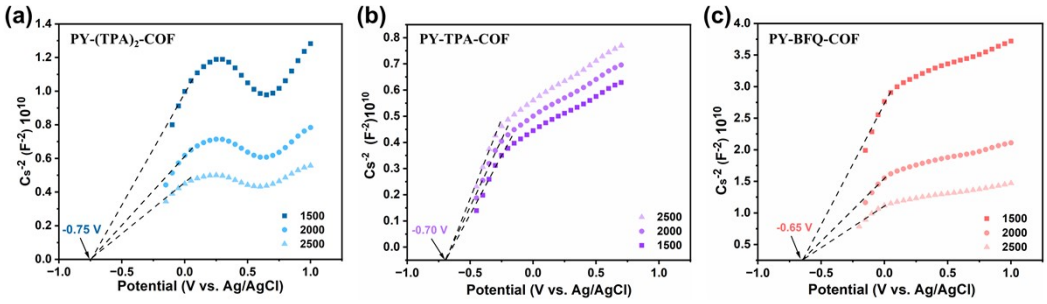

**Figure S15.** Time-resolved transient PL lifetime curves of (a) PY-$(TPA)_2$-COF, (b) PY-TPA-COF, and (c) PY-BFQ-COF.

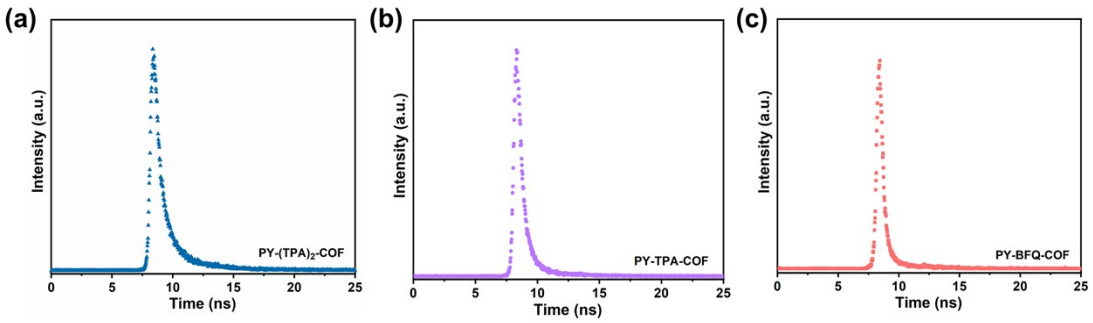

**Figure S16.** $H_2$ evolution of PY-$(TPA)_2$-COF with different photocatalyst masses.

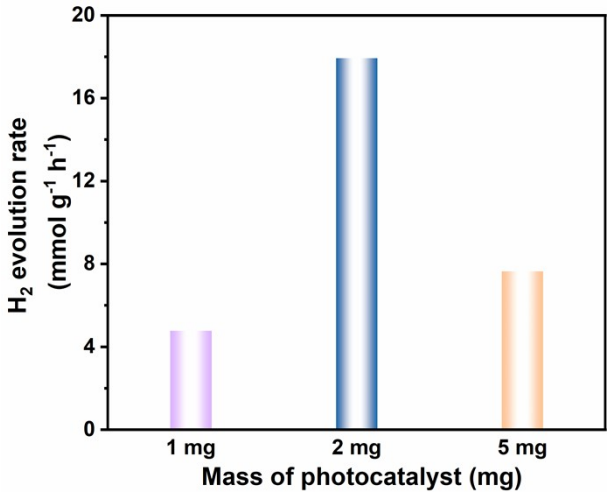

**Figure S17.** Durability measurements of PY-$(TPA)_2$-COF in pure water.

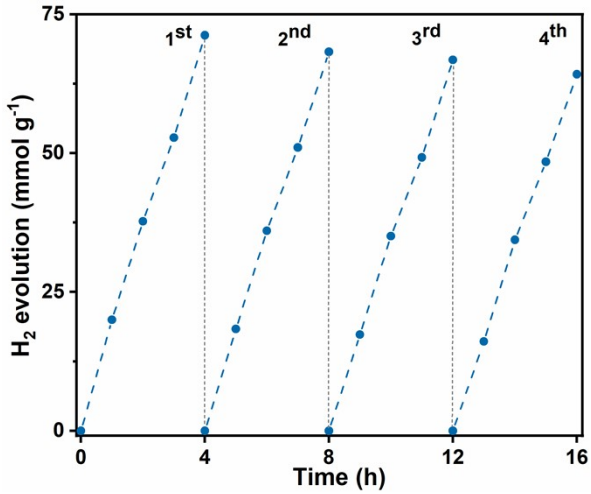

**Figure S18.** SEM images of PY-$(TPA)_2$-COF (a) before and (b) after the photocatalytic reaction in pure water.

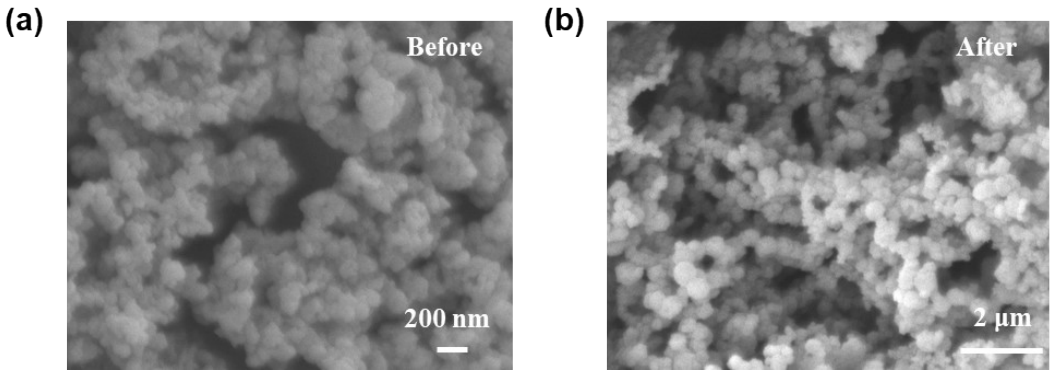

**Figure S19.** (a) XRD patterns and (b) FT-IR spectrum of PY-$(TPA)_2$-COF before and after the photocatalytic reaction in pure water.

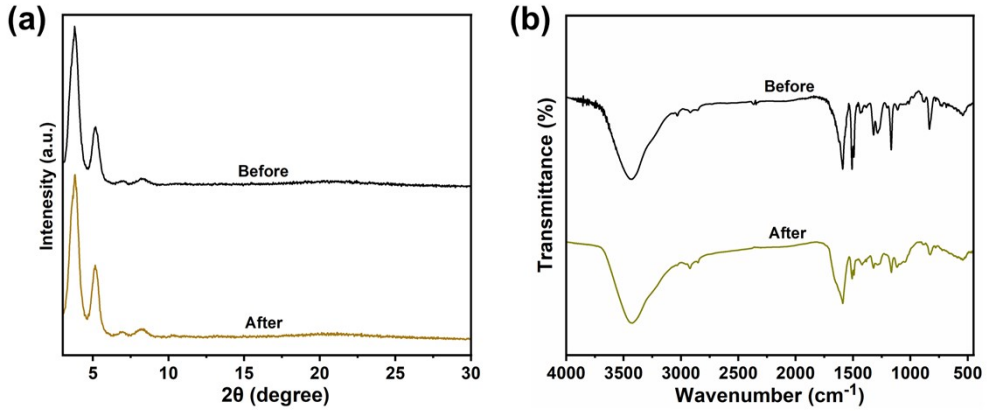

**Figure S20.** XPS spectra of PY-$(TPA)_2$-COF before and after the photocatalytic reaction in pure water: (a) Survey scan, (b, c) N 1s spectra.

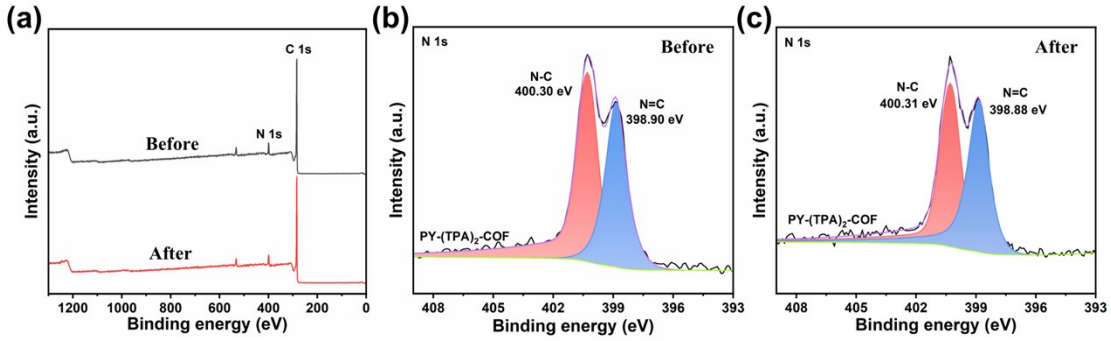

**Figure S21.** The reusability of PY-$(TPA)_2$-COF for photocatalytic $H_2$ evolution in 0.10 M NaCl simulated seawater.

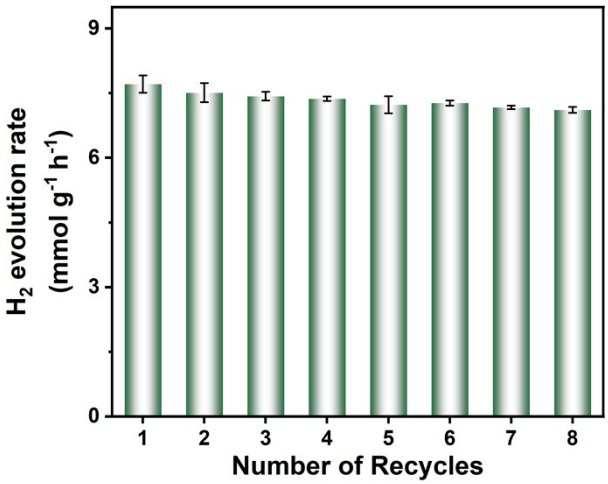

**Figure S22.** SEM images of PY-$(TPA)_2$-COF (a) before and (b) after the photocatalytic reaction in 0.10 M NaCl simulated seawater.

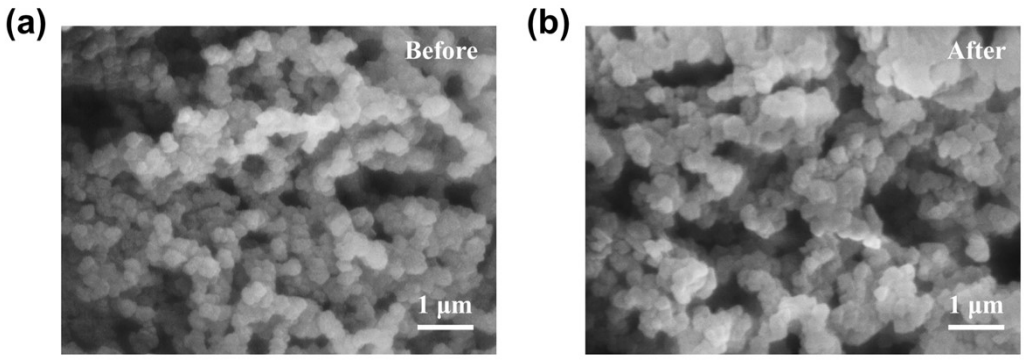

**Figure S23.** FT-IR spectrum of PY-$(TPA)_2$-COF before and after the photocatalytic reaction in 0.10 M NaCl simulated seawater.

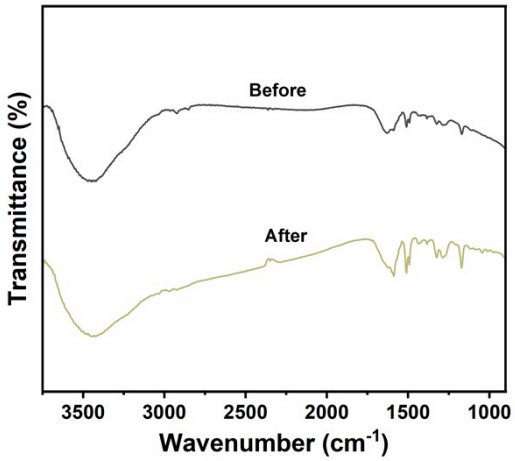

**Figure S24.** Photocatalytic $H_2$ evolution performance of PY-$(TPA)_2$-COF in natural seawater.

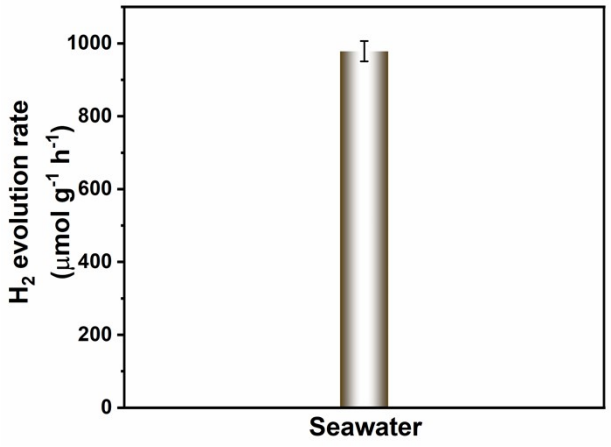

**Figure S25.** Structural diagram of the adsorption of H by (a) PY-$(TPA)_2$-COF, (b) PY-TPA-COF, and (c) PY-BFQ-COF.

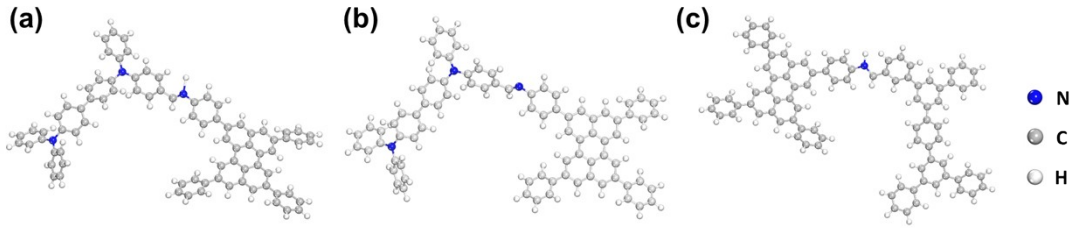

**Figure S26.** Free energy diagram of PY-$(TPA)_2$-COF, PY-TPA-COF, and PY-BFQ-COF for photocatalytic $H_2$ production.

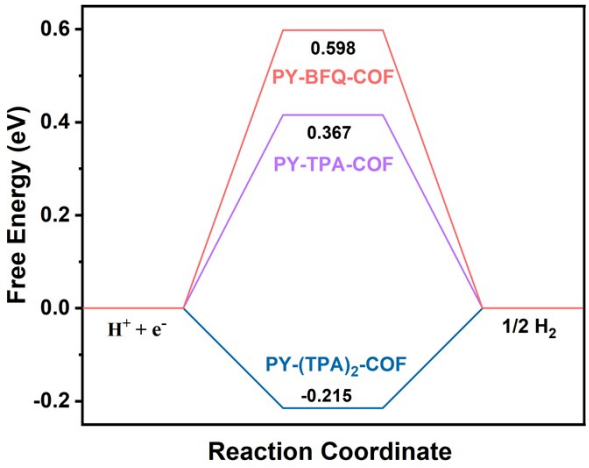

## Section 3. Supporting Tables

**Table S1.** Elemental analysis of PY-$(TPA)_2$-COF, PY-TPA-COF, and PY-BFQ-COF.

| Samples | | N (%) | C (%) | H (%) |
|---|---|---|---|---|
| **PY-$(TPA)_2$-COF** | **Calcd.** | 6.70 | 83.42 | 4.48 |
| | **Found** | 6.84 | 83.26 | 4.40 |
| **PY-TPA-COF** | **Calcd.** | 5.54 | 84.42 | 4.63 |
| | **Found** | 5.42 | 84.66 | 4.70 |
| **PY-BFQ-COF** | **Calcd.** | 3.17 | 75.16 | 4.76 |
| | **Found** | 3.08 | 74.96 | 4.72 |

**Table S2.** Photocatalytic $H_2$ evolution rates in PY-$(TPA)_2$-COF compared to representative COFs and oter materials.

| Catalyst | Cocatalyst | Sacrificial agent | Light Source | Activity (mmol $g^{-1}$ $h^{-1}$) | Ref. |
|---|---|---|---|---|---|
| PY-$(TPA)_2$-COF | Pt | ascorbic acid | Xe light (> 420 nm) | 17.93 | **This work** |
| TAB-TFP-COF | Pt | ascorbic acid | Xe light (> 420 nm) | 1.14 | 5 |
| 10%BiOBr/TpBD-COF | Pt | ascorbic acid | Xe light (≥ 420 nm) | 16.17 | 6 |
| CdS-COF | Pt | ascorbic acid | Xe light (> 420 nm) | 15.10 | 7 |
| CdS | Pt | ascorbic acid | Xe light (> 420 nm) | 6.7 | 7 |
| CTF | Pt | TEOA | Xe light (> 420 nm) | 5.55 | 8 |
| 5%P-COF-1/CTF | Pt | TEOA | Xe light (> 420 nm) | 14.10 | 8 |
| BT-COF | Pt | ascorbic acid | Xe light (> 420 nm) | 7.70 | 9 |
| 30%PEG@BT-COF | Pt | ascorbic acid | Xe light (> 420 nm) | 11.14 | 9 |
| TaTp-COF | Pt | ascorbic acid | Xe light (≥ 420 nm) | 0.74 | 10 |
| TPCBPB-COF | Pt | TEOA | Xe light (> 420 nm) | 1.03 | 11 |
| Ti-MOF/COF | Pt | ascorbic acid | Xe light (= 400 nm) | 13.98 | 12 |
| BD-COF | Pt | ascorbic acid | Xe light (> 420 nm) | 1.98 | 13 |
| $Au_1Cu_5$/COF-TpPa | - | ascorbic acid | Xe light (≥ 420 nm) | 8.24 | 14 |
| Macro-TpBpy | Pt | TEOA | Xe light (> 420 nm) | 4.88 | 15 |
| Py-DNII-COF | Pt | ascorbic acid | Xe light (≥ 420 nm) | 0.63 | 16 |
| AA-TAPT-COF 5% | Pt | TEOA | Xe light | 20.36 | 17 |

**Section 4. References**


1 B. Delley, *J. Chem. Phys.*, 2000, **113**, 7756−7764.

2 B. Delley, *Phys. Rev. B: Condens. Matter Mater. Phys*, 2002, **66**, 155125.

3 J. P. Perdew, K. Burke, M. Ernzerhof, *Phys. Rev. Lett.*, 1996, **77**, 3865−3868.

4 S. Grimme, *J. Comput. Chem.*, 2006, **27**, 1787−1799.

5 X. Wu, M. Zhang, Y. Xia, C. Ru, P. Chen, H. Zhao, L. Zhou, C. Gong, J. Wu, X. Pan, *J. Mater. Chem. A*, 2022, **10**, 17691−17698.

6 H. Ran, X. Liu, J. Fan, Y. Yang, L. Zhang, Q. Guo, B. Zhu, Q. Xu, *J. Materiomics*, 2025, **11**, 100918.

7 G. Sun, J. Zhang, B. Cheng, H. Yu, J. Yu, J. Xu, *Chem. Eng. J.*, 2023, **476**, 146818.

8 N. Xu, Y. Liu, W. Yang, J. Tang, B. Cai, Q. Li, J. Sun, K. Wang, B. Xu, Q. Zhang, Y. Fan, *ACS Appl. Energy Mater.*, 2020, **3**, 11939−11946.

9 T. Zhou, L. Wang, X. Huang, J. Unruangsri, H. Zhang, R. Wang, Q. Song, Q. Yang, W. Li, C. Wang, K. Takahashi, H. Xu, J. Guo, *Nat. Commun.*, 2021, **12**, 3934.

10 X. Zhao, M. Lei, X. Ma, Y. Li, Z, Jin, *J. Catal.*, 2025, **446**, 116086.

11 S. Altınışık, G. Yanalak, İ. H. Patır, S. Koyuncu, *ACS Appl. Mater. Interfaces*, 2023, **15**, 18836−18844.

12 C.-X. Chen, Y.-Y. Xiong, X. Zhong, P. Lan, Z.-W. Wei, H. Pan, P.-Y. Su, Y. Song, Y.-F. Chen, A. Nafady, S. Uddin, S. Ma, *Angew. Chem. Int. Ed.*, 2022, **61**, e202114071.

13 C. Li, J. Liu, H. Li, K. Wu, J. Wang, Q. Yang, *Nat. Commun.*, 2022, **13**, 2357.

14 W. Yang, J. Zhang, Q. Xu, Y. Yang, L. Zhang, *Acta Phys. Chim. Sin.*, 2024, **40**, 2312014.

15 I. E. Khalil, P. Das, H. Küçükkeçeci, V. Dippold, J. Rabeah, W. Tahir, J. Roeser, J. Schmidt, A. Thomas, *Chem. Mater.*, 2024, **36**, 8330−8337.

16 I. M. A. Mekhemer, M. M. Elsenety, A. M. Elewa, K. D. G. Huynh, M. M. Samy, M. G. Mohamed, D. M. Dorrah, D. C. K. Hoang, A. F. Musa, S-W. Kuo, H-H. Chou, *J. Mater. Chem. A*, 2024, **12**, 10790−10798.

17 J. Du, F. Jin, G. Jiang, X. Ma, Z. Jin, *Appl. Catal. B: Environ.*, 2025, **370**, 125167.